ACSNANO www.acsnano.org

ARTICLE

Live Bacterial Physiology Visualized with 5 nm Resolution Using Scanning Transmission Electron Microscopy

Eamonn Kennedy,[†] Edward M. Nelson,[†] Tetsuya Tanaka,[‡] John Damiano,[§] and Gregory Timp*[,⊥]

[†]Department of Electrical Engineering, [‡]Departments of Chemical Biomolecular Engineering and Biological Science, and [⊥]Departments of Electrical Engineering and Biological Science, University of Notre Dame, Notre Dame, Indiana 46556, United States

[§]Protochips, Inc., Morrisville, North Carolina 27560, United States

Supporting Information

ABSTRACT: **It is now possible to visualize at nanometer resolution the infection of a living biological cell with virus without compromising cell viability using scanning transmission electron microscopy (STEM). To provide contrast while preserving viability, *Escherichia coli* and P1 bacteriophages were first positively stained with a very low concentration of uranyl acetate in minimal phosphate medium and then imaged with low-dose STEM in a microfluidic liquid flow cell. Under these conditions, it was established that the median lethal dose of electrons required to kill half the tested population was LD_{50} = 30 e^-/nm^2, which coincides with the disruption of a wet biological membrane, according to prior reports. Consistent with the lateral resolution and high-contrast signal-to-noise ratio (SNR) inferred from Monte Carlo simulations, images of the *E. coli* membrane, flagella, and the bacteriophages were acquired with 5 nm resolution, but the cumulative dose exceeded LD_{50}. On the other hand, with a cumulative dose below LD_{50} (and lower SNR), it was still possible to visualize the infection of *E. coli* by P1, showing the insertion of viral DNA within 3 s, with 5 nm resolution.**

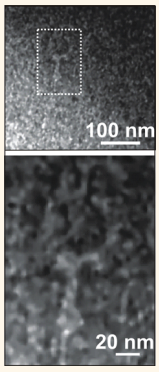

KEYWORDS: *liquid cell, scanning transmission electron microscopy, low-dose biological imaging, E. coli, bacteriophage, infection*

A cell is a wet, living nanosystem. Visualizing the system's physiology demands spatial resolution with a commensurate depth of field on the scale of the protein machinery (3−7 nm) that drives it. Whereas advanced light microscopies promise subdiffraction optics, even in the far-field,[1−3] only *ca.* 40−100 nm has been resolved in (live) cell biology, so far. To relieve these constraints, transmission electron microscopy (TEM) has been employed to image fixed, dehydrated, and stained sections of tissue structure[4,5] or samples at cryogenic temperatures,[6] but not living cells. However, with the introduction of liquid flow cells, imaging biology under hydrated, physiological conditions with TEM has now become practicable.[7−14]

Here, it is demonstrated that living cells can be imaged directly with high resolution (5 nm) using scanning TEM (STEM) in minimal medium without compromising viability. To demonstrate the method, first, the conditions required to *positively* stain *Escherichia coli* (*E. coli*) with uranyl acetate (UA) and the median lethal electron irradiation dose (LD_{50}) required to kill half the tested population were established. Subsequently, the *E. coli* membrane and flagella and the bacteriophage (P1) were visualized with 5 nm resolution. Finally, the infection of *E. coli* by P1 was tracked with high resolution to follow the insertion of the viral DNA. To our knowledge, no other technique has resolved bacterial physiology with this precision. Whereas hydrated cells labeled with gold nanoparticles have been visualized in liquid with STEM to obtain structural information,[11−14] viability was not demonstrated, which is crucial for scrutinizing physiology.

There were several key aspects of this methodology. First, the liquid cell was essential since the chemistry of life patently involves water; more than 70% of cell mass is associated with water. However, thick liquid layers can adversely affect spatial resolution and contrast because multiple scattering broadens the electron beam.[5] On the other hand, if the STEM beam interacts with the biological cell at the top membrane of the liquid cell, before the liquid layer, the beam intensity and contrast may be compromised, but not necessarily the resolution.[4,7,12] Consequently, the top membrane of the liquid cell was coated with poly-L-lysine to promote bacterial adherence to it. Thus, it is the low contrast signal-to-noise ratio (SNR) that limits high-resolution imaging of these biological specimens.[4,5] Although a bright-field emission source, in conjunction with a high-angle annular dark field (HAADF) detector for collecting scattered electrons, can be used to

Received: December 7, 2015
Accepted: January 26, 2016
Published: January 26, 2016

DOI: 10.1021/acsnano.5b07697
ACS Nano 2016, 10, 2669−2677

acquire images with high SNR, the achievable contrast has to be reconciled with the damage induced by electron irradiation of biological specimens.[15−18] In particular, the small scattering cross-section of low atomic number elements (C, O, N, K) that constitute biology translates to a high dose required for an adequate SNR in biological specimens, but the damage threshold for imaging protein in liquid water is low, as low as 1100 e^-/nm^2 at 120 kV for proteins.[17] Provided there is adequate contrast, low-dose imaging, which uses a combination of reduced pixel dwell time and reduced gun current to limit irradiation, can be used with (S)TEM to address this issue and has been used to image abiotic materials with nanometer-scale resolution,[5,18] but has not been used to image live cell physiology, so far. To create contrast, there is a precedent for positively staining whole cell preparations fixed with UA and alcohol for TEM,[19] but if the cells are fixed, the biochemistry stops. It has yet to be established whether live cell physiology can be observed without fixation using UA staining with low-dose beam exposures. We hypothesize that the main limitation on dose is associated with the fragile cell membrane, which consists primarily of phospholipids. For example, the plasma membrane of *E. coli* consists primarily of the lecithin phosphatidylethanolamine. In addition, secondary effects such as the generation of reactive oxygen species and OH^- radical production, which play a causative role in apoptosis,[20,21] may lower the damage threshold even further.

RESULTS AND DISCUSSION

To create contrast, >1% UA has been used widely for negative staining, assuming it does not bind to the specimen. The advantage of UA is that it produces the highest image contrast, but the disadvantage is that it is not indicated for live specimens, as it is toxic at high (≥1%) concentrations. Moreover, the stain precipitates under physiological conditions if there is phosphate in solution. On the other hand, since uranyl ions bind to proteins, lipids, sialic acid carboxyl groups, and the phosphate groups of DNA and RNA, it could be used, potentially, as a positive stain at very low concentration to deliver contrast in membranes,[19] nucleic acids, and proteins without necessarily compromising cell viability or physiology, as indicated by prior work.[22] In addition to a low concentration of UA and a physiological pH, to promote viability and sustain the cell, other environmental factors such as temperature, osmolality, and a culture medium—consisting of amino acids, vitamins, inorganic salts, glucose, serum, and hormones—also have to be taken into account to maintain biological cells.

To satisfy all these requirements, the bacterial *E. coli* strains AW405 and K12 were cultured in a mixture of minimal phosphate-free medium (3-[*N*-morpholino]propanesulfonic acid, MOPS)[23,24] and LB (9:1 MOPS:LB) and maintained at a pH of 7−7.4 in MOPS for imaging. The dilute concentration of LB promotes cell viability in low-phosphate medium, but it retards the growth rate (Figure S1). Subsequently, the *E. coli* cells were positively stained by introducing ≤0.1% UA in MOPS for 30 min just prior to imaging. The optimal conditions for staining with UA that provided contrast without compromising cell viability under the beam were established empirically using both LIVE/DEAD and cell proliferation assays (Figures 1a−f). Whereas aqueous UA stains at 0.01−1% (w/v) were all tested (against 0% UA, which was used as a control), only concentrations at or below 0.1% were consistent with a physiological pH (Figure 1a), which is apparently important since prior work accomplished at low pH showed

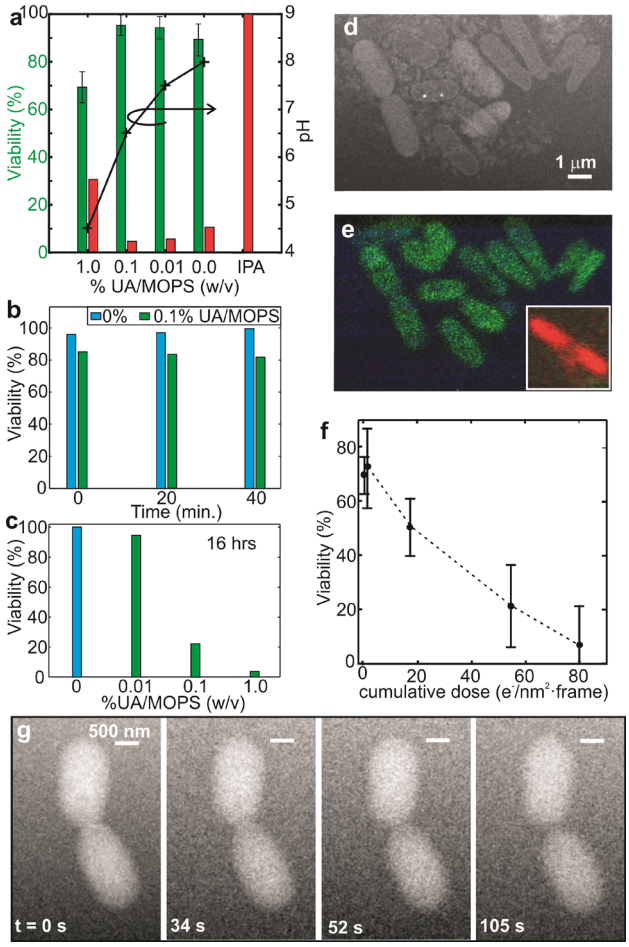

Figure 1. *In situ* STEM imaging of *E. coli* (strain AW405) with high viability. (a) The bar graph shows percent viability scores as a function of uranyl acetate (UA) concentration in MOPS, measured without electron beam irradiation using a LIVE/DEAD assay. The green bars indicate the percentage of live cells, and the red bars denote cells with a compromised membrane. Superimposed on the graph is the corresponding pH (black line, right) as a function of UA concentration in MOPS (w/v). As a control, a culture of the same cells was exposed to isopropyl alcohol (IPA). (b) The bar graph indicates the results of a time-dependent viability analysis of 603 cells by a LIVE/DEAD assay, accomplished in 0% (blue) and 0.1% UA/MOPS (green). The graph shows only a gradual reduction in viability from 86% to 83% over 40 min. (c) A bacterial culture (0.1/mm OD) was exposed for 20 min to the UA/MOPS concentration indicated prior to 20 000× dilution and incubation. The bar graph indicates the number of resulting colonies counted in 16 h. (d) An image of an *E. coli* microcolony stained with 0.1% (w/v) UV/MOPS is shown. The image was acquired in a 2 μm liquid cell at 300 kV acceleration voltage at a magnification of 5000× with a pixel size of 26.7 nm and a dose of 4 e^-/nm^2·frame. (e) Like (d), but the corresponding fluorescence image obtained after LIVE/DEAD assay of the same *E. coli* microcolony (green fluorescence indicates a live cell, while red fluorescence indicates a compromised membrane). (e, inset) An image of two dead cells is shown. (f) Viability is shown as a function of the mean electron beam dose in 0.1% (w/v) UA/MOPS. (g) STEM snapshots of *E. coli* taken at random intervals as indicated, showing binary fission in *E. coli* despite the stain and beam exposure (0.1% (w/v) UA/MOPS, acquired in a 2 μm thick liquid cell at 20 000× with a 6.66 nm pixel and a cumulative dose of <230 e^-/nm^2·frame).

DOI: 10.1021/acsnano.5b07697
ACS Nano 2016, 10, 2669−2677

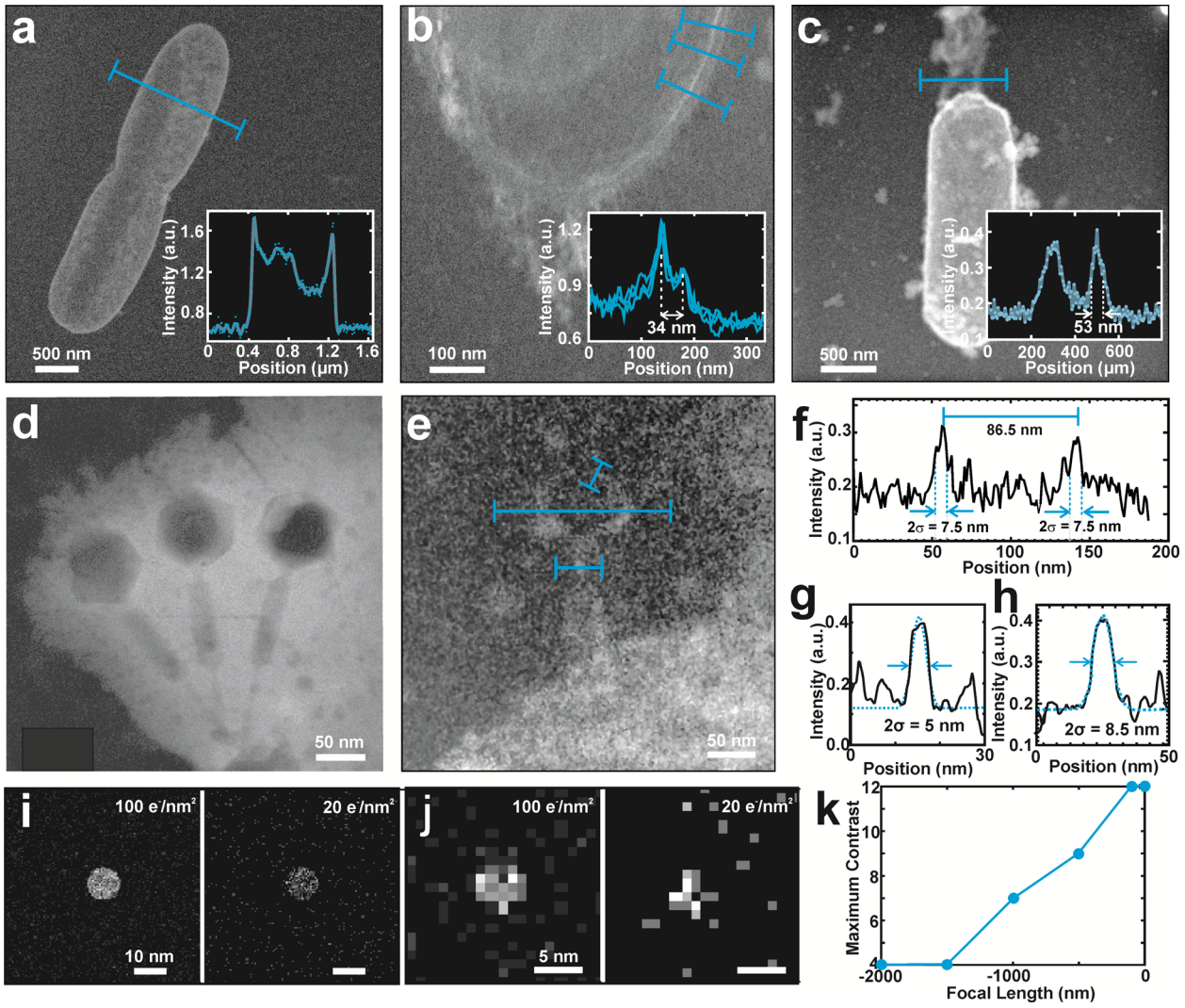

Figure 2. High-resolution HAADF STEM imaging of *E. coli* (strain AW405) membrane and flagella and a P1 bacteriophage on *E. coli* (strain K12). (a) The image shows the results of a resolution test performed in 0.01% (w/v) UA/MOPS, acquired with a cumulative dose of 29 e^-/nm^2·frame. The blue line indicates the position of the line scan (inset). (b) Like (a), but acquired with a cumulative dose of 66 e^-/nm^2·frame. (Inset) The corresponding line scan used to evaluate the contrast and resolution. (c) Image of flagella protruding from *E. coli* stained with 0.1% (w/v) UA/MOPS is shown, which was acquired in a 2 μm thick liquid cell at a magnification of 20 000× with a cumulative dose of 265 e^-/nm^2·frame at 300 kV acceleration voltage. (Inset) The corresponding line scans used to evaluate the contrast and resolution revealing a flagella diameter of 53 ± 2 nm. (d) An image of a negatively stained P1 phage is shown. The phage was deposited on a 50 nm thick silicon nitride membrane and characterized by a capsid measuring ~74 nm wide, a sheath measuring ~105 nm long, and a set of tail fibers. The image was acquired at a magnification of 115 000×, pixel size of 0.42 nm, and cumulative beam dosage of 28 000 e^-/nm^2·frame. (e) An image of a P1 phage adhering to K12 *E. coli* after staining with 0.1% (w/v) UA/MOPS is shown at a 100-fold lower dose than in (d). Like (d), the same structural motifs with practically the same dimensions were apparent for positive UA staining on each phage, including the icosahedral head and contractile tail of P1. The blue lines indicate the position of the line scans shown in (f)−(h). The image was acquired in a 2 μm thick liquid cell at a magnification of 115 000×, pixel dwell time of 3.81 μs, and cumulative beam dosage of 259 e^-/nm^2·frame. (f–h) The corresponding line scans used to evaluate the contrast and resolution revealing that (f) the diameter of the capsid and thickness of the head membrane; (g) the thickness of the head membrane near the top of the capsid; and (h) the thickness of the sheath membrane indicate sub-10 nm resolution. (i) Simulated intensity profile as a function of position under the STEM probe beam for 100 and 20 e^-/nm^2 doses (left, right, respectively), focused at the top of a model of a flow cell containing a U-coated, water-filled 10 nm diameter nanoparticle at the top of a 2 μm thick liquid layer with the beam focused. Regardless of the dose, the 10 nm diameter nanoparticle was clearly resolved with an SNR > 2. (j) Like (i), but the diameter of the nanoparticle was 5 nm instead. The top-focused images were resolved even with a low dose (right, 20 e^-/nm^2) with an SNR ≈ 2. (k) The maximum available contrast as a function of the focus position is shown. Contrast persists even at a depth > 1000 nm.

lower viability.[22] The viability score, measured relative to the control associated with UA staining (without irradiation), revealed no statistically significant loss of viability for concentrations ≤ 0.1%. In particular, the analysis of viability after staining with 0.1% UA without irradiation indicated only a slight reduction in viability to 86% over the control in the short term (35 min), whereas in the long term (16 h), >30% viability was observed for ≤0.1% UA (Figures 1b,c). Furthermore, at ≤1% concentration UA, staining seems to have hardly affected the growth rate, implying that cell physiology was unfazed (Figures S2, S3). Subsequently, the stained bacteria were attached to the silicon nitride membrane constituting the top of

DOI: 10.1021/acsnano.5b07697
ACS Nano 2016, 10, 2669−2677

a standard E-chip. To promote cell adherence, the top membrane was coated with poly-L-lysine. The liquid cell was assembled in the Poseidon sample holder by sealing medium between the top and bottom E-chips. The height of the liquid cell ranged from 150 nm to 2 μm, depending on the E-chip spacer that was used.

After staining with UA, a survey of the conditions for high-resolution imaging was performed. STEM images were acquired from the liquid flow cell with an 80−300 kV FEI Titan TEM using a HAADF detector within about 5−30 min (Figure 1d). To test viability after exposure to the beam, the liquid flow cell was removed from the microscope and a LIVE/DEAD assay was performed, which scored viability by membrane permeability using green and red fluorescence, respectively (Methods). The fluorescence image of the same microcolony imaged with STEM revealed 70% viability after sustaining a dose of 10 e^-/nm^2·frame, consistent with the control without any exposure to the beam (Figure 1e). In contrast, at a cumulative dose of >70 e^-/nm^2·frame nearly all the cells were dead; that is, viability was reduced to <10% (Figure 1f). Fitting the data to a sigmoidal dose−response curve provided an estimate for the mean lethal dose, LD_{50} = 29.4 e^-/nm^2·frame. This value is consistent with other estimates for disruption of wet biological membranes by an electron beam (~30 e^-/nm^2).[25] Taken altogether, these data indicate that STEM imaging of *E. coli* physiology can be accomplished at 300 kV with a dose of about 30 e^-/nm^2·frame using 0.01−0.1% UA staining in a ≤2 μm gap E-chip without compromising cell viability as measured by membrane integrity.

Further support for this claim was obtained using these conditions to observe fission of *E. coli* (Figure 1g). During prokaryotic fission, the DNA is replicated and then each copy is conveyed to opposite poles of the cell. Subsequently, two new poles are formed near the midline, and fission initiates when a septum forms through invagination of the cell wall from opposite directions along the central plane of the cell. The last stages of fission can be observed in the series of snapshots shown in Figure 1g. These observations signified that cell physiology was not critically impaired by either UA staining or low-dose irradiation. This observation is noteworthy because aspects of cell physiology were observed despite a cumulative dose exceeding LD_{50}; it may indicate that adverse effects of the beam can be healed over time. Moreover, a time-dependent analysis of the growth of an *E. coli* culture and colony formation following exposure to UA corroborate this observation, indicating that, for concentrations ≤ 0.1%, physiology was affected minimally since the growth rate depreciated by only 10% (Figure S3).

Regardless of the electron dose, constrained only by the concentration of UA required for viability, STEM images of *E. coli* and P1 bacteriophages revealed several interesting features that serve to establish the resolution targets. *E. coli* is a Gram-negative bacillus with a cell wall consisting of a layer of peptidoglycan that varies in thickness (5−10 nm) in the periplasmic space (about 22 nm thick) sandwiched between lipid bilayers about 7.5−10 nm thick.[26] Although it was possible to define the silhouette of the bacterium without staining (data not shown), the contrast was deficient for resolving the membrane substructure. On the other hand, the structure of the membrane was conspicuous in images acquired with a cumulative dose of about 30 e^-/nm^2·frame or greater obtained from a bacterium stained with ≥0.01% (w/v) UA/MOPS (Figure 2a,b). In particular, at 0.1% UA, with a cumulative dose of 66 e^-/nm^2·frame at 300 kV in a 2 μm thick liquid cell, the nanostructure of the membrane surrounding the cell was resolved into two bands—the outer and cytoplasmic membranes—about 34 nm apart (Figure 2b, inset). The bright−dark line resolution was approximately 14 ± 2 nm. Generally, it was observed that the membrane thickness varied (even for the same bacteria), undulating between 8 and 18 nm, which likely reflects the actual biology.

Under similar conditions, flagella protruding from the *E. coli* membrane (Figure 2c, arrows) and cell motility were also observed. The AW405 strain of *E. coli* is motile; it is a peritrichous bacterium, propelled by several helical flagellar filaments. The flagella have a rigid structure constituted from flagellin that is anchored in the outer membrane of the cell and extends beyond the length of the cell body.[24] The flagellin forms a hollow tube less than 17−20 nm in diameter. Consistent with these representations, the motion of *E. coli*, adhering to the nitride membrane in the liquid cell, was observed for doses < LD_{50} (see supplemental Video V1). The *E. coli* tumbled randomly at about >0.09 Hz, but considering the very low frame rate, this only imposed a lower bound, which is otherwise consistent with reports that indicate tumbling at ~2.5 Hz.[27] The average diameter of a flagellum observed with STEM was 53 ± 2 nm (Figure 2c, inset). These measurements of the flagella diameter were corroborated by AFM topographs acquired in either air or distilled water on similar cells adhering to a mica surface (Figure S4). It was necessary to erode the AFM topographs to account for the volume of the tip (nominally a 2 nm radius silicon tip with a cone angle of about $2\alpha = 56°$) introducing appreciable error into the raw estimate of the flagella width, 52 ± 5 nm, which coincidently was about the diameter inferred from STEM. However, the height of the flagella above the mica was measured at 15 ± 2 nm, which was a more accurate appraisal and consistent with prior reports of the diameter.[24]

Probably due to its close proximity to the silicon nitride membrane and a thin liquid cell, images of a stained P1 bacteriophage revealed the most detail. The P1 bacteriophage of the *E. coli* bacterium is an established virus−host model often used in studies of viral infection and replication. The infection of K12 by P1 was chosen for study because it has already been carefully examined at the nanometer scale using cryo-TEM,[6] and it is among the largest bacteriophages, so it could be visualized easily. P1 is an icosahedral 81−85 nm capsid (although 20% of the heads from virions produced by the same host cells have a diameter of 65 nm) containing a linear double-stranded DNA plasmid 93 601 base-pairs long, with one vertex attached to a contractile tail that ranges in length from 106 to 225 nm and six kinked tail fibers 4−6 nm in cross-section, as apparent from prior work.[6]

To image P1, an active phage was collected as described elsewhere.[28,29] First, as a control, P1 in solution was deposited on a silicon nitride membrane, stained, dried, and then examined with STEM. The nanostructure of a P1 phage was apparent with negative UA staining (Figure 2d). Like prior work,[6] the projection of the capsid measured 74 ± 2 nm across and 80 ± 2 nm from top to bottom; the tail sheath was 93 ± 14 nm long with some evidence of two tail fibers seen using a beam current of 17.2 pA for a cumulative dose of 16 300 e^-/nm^2·frame at 300 kV. The length of the entire tail was estimated to be about 179 nm.

What is new here is that the same size features were observed in viral particles in MOPS adsorbed on *E. coli* (K12) stained

DOI: 10.1021/acsnano.5b07697
ACS Nano 2016, 10, 2669−2677

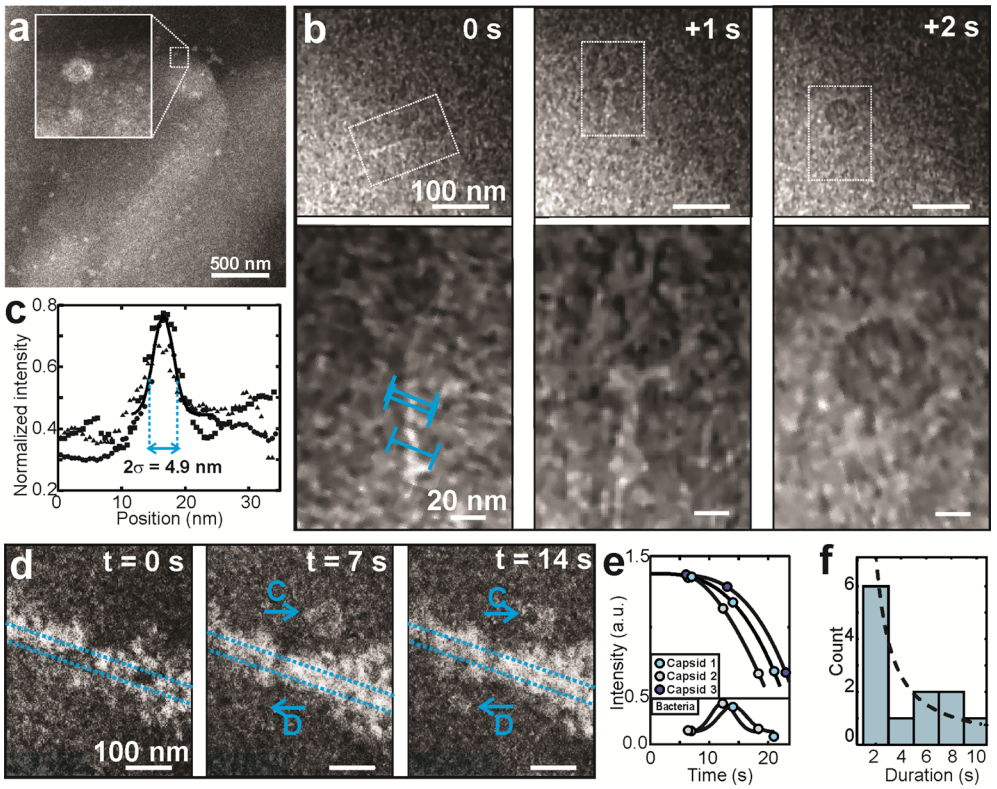

Figure 3. Visualization of P1 bacteriophage infecting live *E. coli* at 5 nm resolution. (a) An image of multiple phages infecting a single bacterium is shown at a dose 4-fold less than LD_{50}. The image was acquired in 0.1% (w/v) UA/MOPS at 20 000× with a cumulative dose of 7.9 e/nm^2·frame. (Inset) Magnified view of a single P1 phage absorbed on *E. coli*. (b) Time lapse (processed) images of a single phage absorbing onto an *E. coli* over a 2 s interval is shown. Cropped insets of the phage are shown below each image. The images acquired at t = 1 and 2 s evince contractile movement of the sheath, indicative of the infection process. The blue lines indicate the position of line scans shown in (c). (c) Corresponding line scans through the stem of the phage shown at 0 s in (b), indicating a 5 nm resolution at low dose. (d) Time-lapsed images, acquired with 0.1% (w/v) UA/MOPS with a dose of 15.7 e/nm^2·frame, showing changes in the intensity of the capsid and internal bacteria over a 14 s interval indicative of the infection process. The dotted blue lines offer a guide, indicating a membrane layer thickness of 35 nm. The blue arrows highlight the intensity attributed to the capsid (C) and DNA (D). The decreasing intensity in the capsid and increasing intensity within the bacteria between t = 7 and 14 s are attributed to the translocation of the viral DNA. After 21 s, the DNA dispersed in the bacteria (data not shown). (e) Measurements of the average intensity in the capsid and bacteria for three infections. (f) Histogram of observed maximum infection durations illustrates that 50% of infecting phages (n = 12) detach in under 2 s.

with 0.1% (w/v) UA/MOPS in a nominally 2 μm thick liquid cell (Figure 2e), although the contrast was degraded and the dose was too high to ensure viability. Without irradiation, with or without UA staining (Figure S2), exposure of *E. coli* to the P1 resulted in a significant loss of optical density (OD_{600}) over 4 h, which likely indicates that cell lysis occurs and the physiology was intact even after positive staining with a low concentration of UA. The interaction between P1 and K12 can clearly be observed during all stages of infection at 0.1% UA concentration (Figure S5). Similar to the dry control, for images acquired in liquid at a dose of 76 e$^-$/nm^2·frame, the capsid measured 72 ± 3 nm across and 86 ± 3 nm top to bottom, and the tail sheath was 107 ± 3 nm long (Figure 2e–h). Although the practical resolution was limited by the SNR, the thickness of the capsid membrane, 8 ± 2 nm on the sides and 5 ± 2 nm at the top of the head (Figure 2f,g), and the neck of the sheath walls, 9 ± 2 nm, could be resolved (Figure 2h), which were consistent with estimates of the head membrane thickness (12.5 nm) and the width of the tail sheath wall (about 4 nm thick) obtained from cryo-TEM (with 1.5 nm resolution) on structurally similar T4 phages.[30−32]

The thickness of the liquid between the nitride membranes evidently affects the contrast and SNR appreciably, but not necessarily the resolution, which was in accord with Monte Carlo simulations (CASINO v3.2) of uranium-coated, water-filled nanoparticles accomplished in a 2 μm thick water layer at 300 keV with a Gaussian beam at a 10 mrad semiangle for a 20−100 e$^-$/nm^2 dose (Figure 2i,j). Similar to prior work on Au nanoparticles,[33] these simulations indicated that nanometer (5 nm) resolution was possible with a U-coated nanoparticle, even if the liquid layer was micrometers thick, provided that the specimen was affixed to the top membrane of the liquid cell. Moreover, the contrast remained even when the cumulative dose was reduced from 100 to 20 e$^-$/nm^2 with the focus −1000 nm (Figure 2k) from the top surface, indicating the resolution targets established above LD_{50} might be achieved with a lower dose without compromising viability. Additionally, to improve contrast and pursue the high resolution, the simulations also revealed that imaging should be accomplished near the edges of the chip where the nominally 2 μm thick liquid cell was 180 nm thinner. The 90 nm flexure in the top membrane of the liquid cell loaded with fluid was measured directly with AFM (Figure S6). Finally, although it was not tested here,[17] besides water, another limitation is scattering from the silicon nitride window, which reduces the SNR. If the Z-contrast is derived from the elastic scattering cross-section, which scales according to $Z^{3/2}$,

DOI: 10.1021/acsnano.5b07697
ACS Nano 2016, 10, 2669−2677

then 50 nm of Si_3N_4 (Z = 10.6) is nearly equivalent to 165 nm of water (Z = 4.8).[17] It should be practical to reduce the nitride membrane thickness from nominally 50 nm to approximately 10 nm to gain resolution provided the window is appropriately reinforced with thicker ribs. Alternatively, graphene could be used instead of silicon nitride.[34]

To punctuate this effort, the infection of *E. coli* by P1 was visualized with STEM, now constrained by *both* the concentration of UA and the electron dose required to maintain viability. What makes this especially interesting is that the precise mechanism by which P1 viral DNA enters the host cell is not understood, mainly because the transient molecular interactions between bacteriophages and bacteria have been difficult to study by conventional approaches.[6,28,29] Prior work tracking single virions on live cells has indicated that virus mobility and subsequent capture by a membrane receptor depend on the lipid environment and receptor aggregation into nanometer-scale domains.[35,36] However, P1 adsorbs to a terminal glucose of the lipopolysaccharides (LPS) core found prevalently in the outer membrane of Gram-negative bacteria.[6,37,38] Ostensibly, the phage particle adsorbs onto the surface of the bacterium using the tail fibers, and then the tail sheath contracts from 225 nm to 105 nm (with DNA or 90 nm without) and the DNA is injected into the host. Significant movement of the P1 base-plate away from the cell surface during tail contraction, from ∼53 nm to ∼100 nm,[6] is also expected. Once it infects the host, the linear DNA circularizes by homologous recombination.[29]

Using a 0.1% UA in a 2 μm liquid cell for optimum contrast and a dose of 8.5 e^-/nm^2·frame at 300 kV, it was possible to analyze the infection process of a single cell over an interval much shorter than the 15 min incubation time required for activation of the P1 in the bacterium.[29] The phage adsorbed onto the surface of the bacterium, typically at multiple locations (Figure 3a), likely because of the prevalence of LPS. Focusing on a single phage (Figure 3a, inset; and b), the phage−cell complex could be visualized with high (5 nm) resolution (Figure 3c) even at a dose less than LD_{50}. Time-lapsed images of a single phage acquired with a dose of 15.7 e^-/nm^2·frame showed the contractile movement of the sheath. Within 3 s, the tail sheath contracted from about 79 nm to about 24 nm above the cell wall, although this measure may be foreshortened due to the orientation of the phage. Evidently, the UA stain offers sufficient contrast for protein and lipids, and it likely does the same for DNA (Figure S7) also, but there was no evidence of DNA in the capsid in this case.

On the other hand, indicative of the infection process, time-lapsed STEM images, acquired with 0.1% (w/v) UA/MOPS with a dose of 15.7 e^-/nm^2·frame, did show changes in the intensity of the capsid and internal bacterium over 21 s (Figure 3d). Prior to 7 s, no clear evidence of scattering above or below the cell membrane was discerned. However, between +7 and +14 s, the intensity in the capsid decreased and the intensity increased within the bacteria, which were attributed to the translocation of the viral DNA. It was presumed that the DNA was dispersed in the bacteria after +21 s. Support for this interpretation of the images was gleaned from the size of the region of interest (ROI) attributed to DNA. Taking the mean hydrodynamic radius of the atoms constituting the base-pairs as 0.28 nm, the volume of the DNA should be about 7×10^5 nm^3, and the associated diameter of a sphere with that volume would be about 110 nm, which is consistent with the measured diameter of the ROI.[39] Moreover, this process in which the capsid and bacterium exchange intensity was observed repeatedly, although the time interval varied (Figure 3e) since the exposure to the beam was limited by LD_{50}. A histogram of duration of the infection illustrated that the majority occur in less than 2 s (Figure 3f). Thus, STEM imaging revealed the structural dynamics, consistent with cryo-TEM,[4] as well as the physiology of the P1 infection of *E. coli* with high resolution as it develops in a time interval of <45 s. This is the first report of high, nanometer-resolution imaging of a biological process with low-dose STEM.

CONCLUSIONS

In summary, using low-dose STEM in conjunction with positive staining by a very low concentration of UA, the physiology of live *E. coli* and its bacteriophage P1 were visualized with high resolution in a liquid flow cell. To ensure viability as indicated by cell proliferation and LIVE/DEAD assays, the stain was limited to ≤0.1% (w/v) UA/MOPS, and the maximum electron dose for viability at 300 kV was less than the median lethal dose, LD_{50} = 30 e^-/nm^2·frame. It is likely that LD_{50} reflects a compromised membrane. Under these conditions, the dynamics of infection of the K12 *E. coli* strain by P1 were directly imaged; features as small as 5 nm were observed. Although UA concentrations of ≥0.1% (w/v) UA/MOPS and electron doses higher than LD_{50}, cell physiology were employed in this effort, they may adversely affect cell viability. Thus, the low-dose imaging methodology developed here cracks open a window into biology through which cell physiology can be revealed with nanometer resolution. Although the margin for imaging is narrow, it is important because the main challenge confronting the system's physiology right now is to create a model of an organism supported by high-precision empirical data that reveals how life functions. This methodology addresses this challenge.

METHODS/EXPERIMENTAL SECTION

Culture of *E. coli* and P1 Bacteriophage. Briefly, following prior work,[23,24] the *E. coli* strain AW405 (CGSC #7707) was cultured at either 30 or 37 °C overnight in low-phosphate medium, potassium morpholinopropane sulfonate (MOPS) until the log-growth phase was observed ($OD_{633\ nm}$ 0.2), washed with MOPS at pH 7.4−7.8 media, centrifuged (2300 rcf, 5 min), and then resuspended in MOPS. A final wash was performed with 20 mM 3-(*N*-morpholino) propanesulfonic acid containing 5 mM $CaCl_2$ adjusted to pH 7.2 by adding NaOH. If the strain contained a plasmid for antibiotic resistance, the media also included the appropriate antibiotic and the bacteria were cultured at 30 °C to maintain plasmid stability. Otherwise, 37 °C was used.

The MOPS medium was drawn from a 10× concentrate prepared by mixing the following solutions in order to prevent precipitation: 1.0 M, adjusted to pH 7.4 with KOH (400 mL); *N*-tris(hydroxymethyl)-methyl glycine (Tricine), freshly prepared to 1.0 M and filtered. Subsequently, the pH was adjusted to 7.2 with approximately 300 μL of 10 M NaOH. The solution was sterilized and stored at 4 °C for up to 1 month.

Active P1 phages were collected essentially as described elsewhere.[28,29] Briefly, lyophilized wild-type, nonlysogenic *E. coli* K-12 (ATCC #25404) was cultured in LB medium. An overnight culture of *E. coli* K-12 was diluted 100-fold with LB medium and incubated at 37 °C with vigorous shaking (250 rpm) for 3−4 h to obtain a fresh culture at the log phase. Cryo-preserved P1 phages (ATCC 25404-B1) were diluted with LB medium 1:1, which was further mixed with the log-phase culture of *E. coli* 1:50 and incubated at 37 °C for 20 min. This phage−*E. coli* suspension was diluted with LB medium supplemented with 10 mM $CaCl_2$ and 0.5% agarose and poured onto an LB agar plate. After the top agar was solidified, the plate was

DOI: 10.1021/acsnano.5b07697
ACS Nano 2016, 10, 2669−2677

incubated at 37 °C overnight in an upright position. The next day, 10 plaques were picked with Pasteur pipettes, collected into a tube with 30 μL of LB, and stored as an active P1 stock at 4 °C. This active P1 phage stock was mixed with a fresh log-phase culture of *E. coli* K-12 1:50 and incubated at 37 °C for 5 min. This phage−*E. coli* mix was diluted 50-fold with LB with 5 mM $CaCl_2$ and incubated at 37 °C with vigorous shaking for 3 h or until visible cell lysis was observed. This culture was treated with chloroform (10% of a total volume, v/v), vortexed, and mixed with NaCl at the final concentration of 0.5 M. After centrifugation at 7000*g* for 10 min to remove bacterial debris, the supernatant with phage particles was mixed with 6 kDa PEG at the final concentration of 10%. Precipitated phage particles were collected by centrifugation at 10000*g* for 15 min. After the pellet was resuspended into TM buffer (10 mM TrisHCl pH 7.4, 100 mM NaCl, and 10 mM MgCl2) at 4 °C overnight, this suspension was mixed with chloroform 1:1 and centrifuged at 5000*g* for 15 min to remove PEG for imaging.[40]

Positive Staining of *E. coli* and P1 Phage with Uranyl Acetate. Aqueous uranyl acetate (Ted Pella) was prepared from a 5% (w/v) stock solution, filtered with a Whatman #1 filter into a 200 mL brown bottle (for protection against light), and stored at 4 °C. Just prior to use it was filtered again with a 0.2 μm porous filter. The stock solution was diluted further prior to staining. Typically, for the concentrations used for staining 50 μL of 1% UA was added to 450 μL of low-phosphate culture (0.1% w/v UA) at ODs of about 0.25 (~2×10^8 cells/mL) and then incubated for 10 min and stored in the dark in a shaker agitating the suspension at 290 rpm. Corresponding to the liquid cell volume, this meant about 10−100 bacteria could be imaged at one time.

To test viability in UA, five samples were collected and incubated for 1 h: one containing just MOPS (control), 1%, 0.1%, and 0.01% (w/v) UA/MOPS, as well as a 50% (v/v) 2-propanal/MOPS for a negative control. Likewise, to test sensitivity to the electron dose, five samples were collected, stained with 0.1% UA/MOPS, incubated for 90 min, and then exposed to five electron doses ranging from 2.5 to 75 e^-/nm^2·frame. Analyses of the time dependence of viability, growth, and physiology after exposure to UA stain are done with and without irradiation (Figures 1 and S1−3).

Fluorescence Microscopy and LIVE/DEAD Assay. Fluorescence microscopy was used to score cell viability after exposure to UA and the electron beam dose. The bacteria were stained according to the bacterial LIVE/DEAD assay (BacLight, Life Technologies, CA, USA) protocol supplied by the manufacturer, which uses membrane-permeant SYTO 9 labels to report live bacteria with green fluorescence and membrane-impermeant propidium iodide (PI) to identify membrane-compromised bacteria with red fluorescence. SYTO 9 penetrates the bacterial cell membrane and binds to nucleic acids in both live and dead cells, whereas PI penetrates the cell membrane and intercalates into nucleic acids only if the membrane is compromised (*i.e.*, when a cell dies). When SYTO 9 and PI are mixed and applied to a dead cell, PI preferentially binds to nucleic acids, such that SYTO 9 (green) fluorescence weakens and PI (red) fluorescence predominates.

The fluorescence data were collected using a Leica TCS SP5 II (Leica Microsystems) confocal microscope with enhanced, hybrid GaAsP detectors for improved sensitivity to fluorescence. All confocal images were acquired using an HCX PL APO lambda blue 63× 1.2 NA (Leica) water immersion objective using a 488 nm argon excitation laser at a power of 500 nW for the LIVE and 543 nm HeNe excitation for the DEAD assays.

Liquid Flow Cell. All the STEM imaging was performed in a Poseidon 210 *in situ* liquid cell TEM flow holder (Protochips Inc., Morrisville, NC, USA). The holder was designed to accommodate a microfluidic liquid cell in the vacuum of the electron microscope. The microfluidic liquid cell was assembled using a standard flat E-chip, sandwiched together with Gap-Set E-chips ranging from 150 nm to 2 μm (EPT-52W, EPT-52Q, EPB-52F, Protochips). The liquid cell has transparent windows fabricated from low-pressure CVD silicon nitride, nominally 50 nm thick with open membranes spanning an area of 500 × (20−50) μm^2. Prior to loading, the E-chips were cleaned with acetone, ethanol, and (18 MΩ) deionized water, blown dry with dry nitrogen gas, and then subjected to a 25 W oxygen plasma (Harrick Plasma, Ithaca, NY, USA) at 1.2 Torr for 1 min. The top E-chip was subsequently coated with a thin layer of 0.01% v/v poly-L-lysine (Ted Pella) (0.1 monolayer thick) to make the windows hydrophilic and promote cell attachment.

The two E-chip components were then fitted into a slot in the STEM/TEM specimen holder with their silicon nitride surfaces facing, such that the silicon nitride windows in the middle of both chips overlapped. For loading of the sample in the fluid holder, O-rings were first added to ensure a hermetic seal of the chamber. A spacer was then placed in the slot of the holder with its silicon nitride surface facing up, and a thin (<1 μL) film of solution containing UA-stained P1−K12 complex was pipetted onto its top side. Immediately afterward, the "top" E-chip, coated with stained, adhering bacteria solution, was placed face down on the spacer chip, forming the liquid cell. In this way, the silicon nitride surfaces of both chips were kept under MOPS medium continuously. The fluid holder was closed with a cover lid, and excess solution was carefully removed from its exterior edges using filter paper. The holder was then tested for leaks, and its exterior was cleaned under oxygen plasma for 5 min.

STEM. *In situ* STEM images were acquired using an 80−300 kV FEI probe Titan transmission electron microscope (Titan 80/300, FEI, Hillsborough, OR, USA) using a high-angle, annular dark field detector (Fischione Instruments, Export, PA, USA) with a semiangle of 50 mrad. This instrument was equipped with a field emission gun operated at a 3950 V extraction voltage and a 300 kV acceleration voltage. A 50 μm condenser aperture was used to reduce the flux of electrons incident on the sample. The spot size ranged from a setting of 8 to 9, typically. Imaging commenced by locating the edge of the nitride window in a fast scanning search mode.

To control the electron dose during image acquisition, the pixel dwell time (*i.e.*, increasing the STEM scanning speed) was reduced. STEM images were recorded with 512 × 512 pixel resolution at room temperature using TIA software (Philips/FEI, Delft) with a pixel dwell time that ranged from 4 to 20 μs and a pixel size ranging from 0.42 nm magnification (115 000×) to 26.65 nm (magnification 5000×). Finally, the images were imported into MATLAB (Natick, MA, USA), where the contrast was adjusted so that the top and bottom 1% of the pixel intensity was saturated and then converted into bitmaps.

To enhance the visibility of the stained structures, the images were filtered with a 2D Wiener filter and a 2D median filter with contrast reset as before. The pixel size of the filter varied with the magnification used (typically 3−5 pixels). For low-dose imaging, the gamma level was set to 0.75, and the contrast level and brightness were adjusted for maximal visibility of the membrane (Adobe Photoshop, Adobe, San Jose, CA, USA).

Monte Carlo Simulations of STEM Resolution. The trajectories of the scattered electrons in STEM were simulated with the CASINO (v3.2) Monte Carlo simulation package.[33] The flow cell was modeled as a 2 μm thick water layer sandwiched between two 50 nm thick Si_3N_4 layers with a 5−10 nm diameter U coated, water-filled sphere placed at defined locations inside the cell. The electron probe was modeled as a 300 keV Gaussian beam (σ = 1.28) with a diameter of 1 nm and a 10 mrad semiangle. Noise was added to the detector signal to simulate shot noise. The trajectories of 20−100 electrons were calculated, while the probe beam was scanned in 1 nm steps over the model cell from which a simulated image emerged.

Topography Measured with AFM. The topography of *E. coli* flagella and the flexure in a filled liquid cell were measured using a customized AFM (MFP-3D-BIO, Asylum Research, Santa Barbara, CA, USA) interfaced to an inverted optical microscope (Axio-Observer Z1, Zeiss). *E. coli* were attached to a freshly cleaved piece of mica. Poly-L-lysine (PLL, Ted Pella) was first deposited on the mica and then incubated for 30 min. The coated mica was subsequently rinsed in 18 MΩ deionized water and dried with flowing nitrogen gas. The *E. coli*, harvested in MOPS as described above, were then deposited on the PLL-coated mica and incubated for 30 min before the mica was gently rinsed with distilled water and dried under flowing nitrogen gas. The *E. coli* were then imaged in distilled water in noncontact (tapping) mode with a custom-made, sharp (nominally 2

DOI: 10.1021/acsnano.5b07697
ACS Nano 2016, 10, 2669−2677

nm diameter and a cone angle of about $2\alpha = 56°$) silicon tip with a nominally soft spring constant (k = 600 pN/nm) cantilever (MSNL with the metallic backside removed, Bruker, Fremont, CA, USA). The cantilever was positioned directly above a cell using a 40× telescope and then scanned at a low line-scan rate (0.1 Hz).

The topography of the silicon nitride membranes comprising the liquid cells was imaged similarly. The roughness and flexure of the membrane were measured by AFM in noncontact (tapping) mode using silicon probes (PPP-NCHR, Nanosensors, Neuchatel, Switzerland). The images were processed with a Gaussian low-pass filter (100 × 100 pixels) with a standard deviation of 0.5 to suppress noise and then converted to a binary map with a threshold of >0.75 nm to calculate the area.

ASSOCIATED CONTENT

Supporting Information

The Supporting Information is available free of charge on the ACS Publications website at DOI: 10.1021/acsnano.5b07697.

Figures showing the influence of low-phosphate media on growth rate; time-dependent analyses of colony growth in 0.01% UA; the physiology and growth of *E. coli* after exposure to UA stain; an AFM profile of *E. coli* flagella; the infection, in real time, of live *E. coli* at sub-10 nm resolution; the liquid thickness variation across a membrane; and UA-stained DNA in a P1 capsid (PDF) (AVI)

AUTHOR INFORMATION

Corresponding Author

*E-mail: gtimp@nd.edu.

Notes

The authors declare the following competing financial interest(s): J. Damiano is the CTO of Protochips, Inc. Protochips Inc. manufactures the Poseidon 210 sample holder used in this work.

ACKNOWLEDGMENTS

We thank Dr. Sergei Rouvimov for assistance with (S)TEM in the bioimaging facility at Notre Dame. This work was supported by SBIR Phase II, 5R44EB008589-04 award from the NIH "Flowcell for biological imaging with liquid TEM", the Walther Cancer Foundation, and a Keough-Hesburgh professorship.

REFERENCES

(1) Willig, K. I.; Kellner, R. P.; Medda, R.; Hein, B.; Jakobs, S.; Hell, S. W. Nanoscale Resolution in GFP-Based Microscopy. *Nat. Methods* **2006**, *3*, 721−723.

(2) Yuan, G.; Rogers, E. T. F.; Roy, T.; Adamo, G.; Shen, Z.; Zheludev, N. I. Planar Super-oscillatory Lens for Sub-Diffraction Optical Needles at Violet Wavelengths. *Sci. Rep.* **2014**, *4*, 6333.

(3) Kennedy, E.; Al-Majmaie, R.; Zerulla, D.; Al-Rubeai, M.; Rice, J. H. Nanoscale Infrared Absorption Imaging Permits Non-Destructive Intracellular Photosensitizer Localization for Subcellular Uptake Analysis. *RSC Adv.* **2013**, *3*, 13789.

(4) Reimer, L.; Kohal, H. *Transmission Electron Microscopy Physics of Image Formation*; Springer: New York, NY, 2008.

(5) Carlson, D. B.; Evans, J. E. Low-Dose Imaging Techniques for Transmission Electron Microscopy. In *The Transmission Electron Microscope*; Khan, M., Ed.; Intech, 2012.

(6) Liu, J.; Chen, C.-Y.; Shiomi, D.; Niki, H.; Margolin, W. Visualization of Bacteriophage P1 Infection by Cryo-electron Tomography of Tiny *Escherichia coli*. *Virology* **2011**, *417* (2), 304−311.

(7) Holtz, M. E.; Yu, Y.; Gao, J.; Abruña, H. D.; Muller, D. A. *In Situ* Electron Energy-Loss Spectroscopy in Liquids. *Microsc. Microanal.* **2013**, *19*, 1027−1035.

(8) de Jonge, N.; Ross, F. M. Electron Microscopy of Specimens in Liquid. *Nat. Nanotechnol.* **2011**, *6*, 695−704.

(9) Evans, J. E.; Jungjohann, K. L.; Browning, N. D.; Arslan, I. Controlled Growth of Nanoparticles from Solution with *in situ* Liquid Transmission Electron Microscopy. *Nano Lett.* **2011**, *11*, 2809−2813.

(10) Yuk, J. M.; Park, J.; Ercius, P.; Kim, K.; Hellebusch, D. J.; Crommie, M. F.; Lee, J. Y.; Zettl, A.; Alivisatos, A. P. High-Resolution EM of Colloidal Nanocrystal Growth Using Graphene Liquid Cells. *Science* **2012**, *366*, 61−64.

(11) Peckys, D. B.; de Jonge, N. Visualization of Gold Nanoparticle Uptake in Living Cells with Liquid Scanning Transmission Electron Microscopy. *Nano Lett.* **2011**, *11*, 1733−1738.

(12) de Jonge, N.; Poirier-Demers, N.; Demers, H.; Peckys, D. B.; Drouin, D. Nanometer-Resolution Electron Microscopy through Micrometers-Thick Water Layers. *Ultramicroscopy* **2010**, *110*, 1114−1119.

(13) Peckys, D. B.; Mazur, P.; Gould, K. L.; de Jonge, N. Fully Hydrated Yeast Cells Imaged with Electron Microscopy. *Biophys. J.* **2011**, *100*, 2522−2529.

(14) Huang, T.-W.; Liu, S.-Y.; Chuang, Y.-J.; Hsieh, H.-Y.; Tsai, C.-Y.; Huang, Y.-T.; Mirsaidov, U.; Matsudaira, P.; Tseng, F.-G.; Chang, C.-S.; Chen, F.-R. Self-Aligned Wet-Cell for Hydrated Microbiology Observation in TEM. *Lab Chip* **2012**, *12*, 340−347.

(15) Thach, R. E.; Thach, S. S. Damage to Biological Samples Caused by the Electron Beam during Electron Microscopy. *Biophys. J.* **1971**, *11*, 204−210.

(16) Abellan, P.; Woehl, T. J.; Parent, L. R.; Browning, N. D.; Evans, J. E.; Arslan, I. Factors Influencing Quantitative Liquid (Scanning) Transmission Electron Microscopy. *Chem. Commun.* **2014**, *50*, 4873.

(17) Mirsaidov, U. M.; Zheng, H. M.; Casana, Y.; Matsudaira, P. Imaging Protein Structure in Water at 2.7 nm Resolution by Transmission Electron Microscopy. *Biophys. J.* **2012**, *102*, L15−L17.

(18) Buban, J. P.; Ramasse, Q.; Gipson, B.; Browning, N. D.; Stahlberg, H. High-resolution Low-Dose Scanning Transmission Electron Microscopy. *J. Electron Microsc.* **2010**, *59*, 103−112.

(19) Murray, R. G.; Hall, M.; Thompson, B. G. Cell Division in *Deinococcus radiodurans* and a Method for Displaying Septa. *Can. J. Microbiol.* **1983**, *29*, 1412−23.

(20) Lee, J. H.; Kim, S. Y.; Kil, I. S.; Park, J.-W. Regulation of Ionizing Radiation-induced Apoptosis by Mitochondrial $NADP^+$-dependent Isocitrate Dehydrogenase. *J. Biol. Chem.* **2007**, *282*, 13385−13394.

(21) Daly, M. J.; Gaidamakova, E. K.; Matrosova, V. Y.; Vasilenko, A.; Zhai, M.; Venkateswaran, A.; Hess, M.; Omelchenko, M. V.; Kostandarithes, H. M.; Makarova, K. S.; Wackett, L. P.; Fredrickson, J. K.; Ghosal, D. Accumulation of Mn(II) in *Deinococcus radiodurans* Facilitates Gamma-Radiation Resistance. *Science* **2004**, *306*, 1025−8.

(22) Khemiri, A.; Carrie, M.; Bremond, N.; Ben Mlouka, M. A.; Coquet, L.; Llorens, I.; Chapon, V.; Jouenne, T.; Cosette, P.; Berthomieu, C. *Escherichia coli* Response to Uranyl Exposure at Low pH and Associated Protein Regulations. *PLoS One* **2014**, *9*, e89863.

(23) Neidhardt, F. C.; Bloch, P. L.; Smith, D. F. Culture Medium for Enterobacteria. *J. Bacteriol.* **1974**, *119*, 736−747.

(24) Turner, L.; Ryu, W.; Berg, H. C. Real-Time Imaging of Fluorescent Flagellar Filaments. *J. Bacteriol.* **2000**, *182*, 2793−2801. Darnton, N. C.; Turner, L.; Rojevsky, S.; Berg, H. C. On Torque and Tumbling in Swimming *Escherichia coli*. *J. Bacteriol.* **2007**, *189*, 1756−1764.

(25) Hui, S. W.; Parsons, D. F. Electron Diffraction of Wet Biological Membranes. *Science* **1974**, *184*, 77−78.

(26) Silhavy T. J.; Kahne, D.; Walker, S.; Shapiro, L.; Losick, R. The Bacterial Cell Envelope. *Cold Spring Harbor Perspect. Biol.* **2010**, *2*, a00041410.1101/cshperspect.a000414.

(27) Neuman, K. C.; Chadd, E. H.; Liou, G. F.; Bergman, K.; Block, S. M. Characterization of Photodamage to *Escherichia coli* in Optical Traps. *Biophys. J.* **1999**, *77*, 2856−2863.

DOI: 10.1021/acsnano.5b07697
ACS Nano 2016, 10, 2669−2677

(28) Sternberg, N. L.; Maurer, R. Bacteriophage-Mediated Generalized Transduction in *Escherichia coli* and *Salmonella typhimurium*. *Methods Enzymol.* **1991**, *204*, 18−43.
(29) Werner, E. R.; Christensen, J. R. Infection by Bacteriophage P1 and Development of Host-Controlled Restriction and Modification and of Lysogenic Immunity. *J. Virol.* **1969**, *3*, 363−368.
(30) Bradley, D. E.; Kay, D. The Fine Structure of Bacteriophages. *J. Gen. Microbiol.* **1960**, *23*, 558−562.
(31) Kostyuchenko, V. A.; Chipman, P. A.; Leiman, P. G.; Arisaka, F.; Mesyanzhinov, V. V.; Rossmann, M. G. The Tail Structure of Bacteriophage T4 and Its Mechanism of Contraction. *Nat. Struct. Mol. Biol.* **2005**, *12*, 810−13.
(32) Fokine, A.; Rossmann, M. G. Molecular Architecture of Tailed Double-Stranded DNA Phages. *Bacteriophage* **2014**, *4*, e28281.
(33) Demers, H.; Ramachandra, R.; Drouin, D.; de Jonge, N. The Probe Profile and Lateral Resolution of Scanning Transmission Electron Microscopy of Thick Specimens. *Microsc. Microanal.* **2012**, *18*, 582.
(34) Yuk, J. M.; Park, J.; Ercius, P.; Kim, K.; Hellebusch, D. J.; Crommie, M. F.; Lee, J. Y.; Zettl, A.; Alivisatos, A. P. High-Resolution EM of Colloidal Nanocrystal Growth Using Graphene Liquid Cells. *Science* **2012**, *336*, 61−61.
(35) Kukura, P.; Ewers, H.; Muller, C.; Renn, A.; Helenius, A.; Sandoghdar, V. High-Speed Nanoscopic Tracking of the Position and Orientation of a Single Virus. *Nat. Methods* **2009**, *6*, 923−927.
(36) Alsteens, D.; Trabelsi, H.; Soumillion, P.; Dufrêne, Y. F. Multiparametric Atomic Force Microscopy Imaging of Single Bacteriophages Extruding from Living Bacteria. *Nat. Commun.* **2013**, *4*, 2926.
(37) Sandulache, R.; Prehm, P.; Kamp, D. Cell Wall Receptor for Bacteriophage Mu G(+). *J. Bacteriol.* **1984**, *160*, 299−303.
(38) Edgar, R.; Rokney, A.; Feeney, M.; Semsey, S.; Kessel, M.; Goldberg, M. B.; Adhya, S.; Oppenheim, A. B. Bacteriophage Infection is Targeted to Cellular Poles. *Mol. Microbiol.* **2008**, *68*, 1107−1116.
(39) Fernandes, M. X.; Ortega, A.; Lopez-Martinez, M. C.; Garcia de la Torre, J. Calculation of Hydrodynamic Properties of Small Nucleic Acids from their Atomic structure. *Nucleic Acids Res.* **2002**, *30*, 1782−1788.
(40) Boulanger, P. Purification of Bacteriophages and SDS-PAGE Analysis of Phage Structural Proteins from Ghost Particles. *Methods Mol. Biol.* **2009**, *502*, 227−238.

DOI: 10.1021/acsnano.5b07697
ACS Nano 2016, 10, 2669−2677